Multiconductor Transmission Line Characterization

Dylan F. Williams, *Senior Member, IEEE*

Keywords: Electromagnetic modes, coupling, measurement, microstrip, multiconductor transmission line.

***Abstract*- This paper presents a measurement method that completely characterizes lossy printed multiconductor transmission lines. It determines not only the matrices of impedances and admittances per unit length describing the transmission line in the conductor representation, but also the propagation constants, characteristic impedances, and cross-powers for each mode supported in the line. We apply the method to a pair of lossy coupled asymmetric microstrip lines.**

INTRODUCTION

This paper presents a measurement method that determines all of the modal and "power-normalized" conductor quantities of [1] and [2] describing a multiconductor transmission line. The method eliminates the requirement of [3] that the relationships between the modal and

Reprinted from IEEE Trans. Comp., Pack., and Manuf., Technol.-Part B, vol. 20, no. 2, pp. 129-132, May 1997. Publication of the National Institute of Standards and Technology, not subject to copyright.

conductor voltages be fixed by symmetry conditions and known in advance. We demonstrate this by applying the method to a pair of lossy asymmetric coupled microstrip lines.

The method consists of performing numerous two-port scattering-parameter measurements on multiple lengths of a multiconductor transmission line. In each case we connect the terminals at each of the analyzer measurement ports between one of the conductors of the transmission line and its ground; previously characterized loads connect all of the remaining conductors at both the near and far ends of the line to their grounds. We apply the weighted orthogonal distance regression algorithm of Ref. [4] to find the matrices of transmission line impedances and admittances per unit length that best reproduce the two-port measurements. The procedure places no restriction on the values of terminating impedances, uses all of the available data in an optimal fashion, and can provide error estimates for the results.

We apply the method in several stages. First we verify useful properties without making any assumptions about the line. We then determine the low-frequency limit of the lines capacitance matrix and use these results to resolve the problem with improved accuracy. As discussed in [5], at this final stage of the analysis we can also add a reciprocal error box to the problem to account for the transition parasitics: this may be is useful when the multiconductor transmission lines are embedded in connectors or in a package with significant electrical parasitics.

THE TRANSMISSION-LINE MODES

The total transverse electric field $\boldsymbol{E}_t$ and magnetic field $\boldsymbol{H}_t$ in a closed transmission line that is uniform in z and constructed of linear isotropic materials can be written as [6]

$$\boldsymbol{E}_{\mathrm{t}} = \sum_n \frac{v_{\mathrm{m}n}(z)}{v_{0n}}\, \boldsymbol{e}_{\mathrm{t}n} \;; \quad \boldsymbol{H}_{\mathrm{t}} = \sum_n \frac{i_{\mathrm{m}n}(z)}{i_{0n}}\, \boldsymbol{h}_{\mathrm{t}n}, \tag{1}$$

where $v_{\mathrm{m}n}$ and $i_{\mathrm{m}n}$ are the modal voltages and currents of the nth mode, $\boldsymbol{e}_{\mathrm{t}n}$ and $\boldsymbol{h}_{\mathrm{t}n}$ are its transverse modal electric and magnetic fields (functions only of the transverse coordinates x and y), the sums span all of the excited modes in the line, and the time harmonic dependence $e^{+j\omega t}$, where ω is the real angular frequency, has been suppressed. In open guides we must add a continuous spectrum of modes to this discrete set [7], which we assume that we can neglect.

We restrict the normalizing voltages v_{0n} and currents i_{0n} by $v_{0n} i_{0n}^{*} = p_{0n} \equiv \int_S \boldsymbol{e}_{\mathrm{t}n} \times \boldsymbol{h}_{\mathrm{t}n}^{*} \cdot \boldsymbol{z}\, \mathrm{d}S$, where $\mathrm{Re}(p_{0n}) \geq 0$, so that the power carried in the forward direction by the nth forward and backward modes in the absence of any other modes in the guide is given by $v_{\mathrm{m}n}\, i_{\mathrm{m}n}^{*}$; this is the conventional normalization and corresponds to the power condition used in Refs. [1] and [8] and suggested by Brews [9]. The characteristic impedance of the nth mode is $Z_{0n} \equiv v_{0n}/i_{0n} = |v_{0n}|^2/p_{0n}^{*} = p_{0n}/|i_{0n}|^2$; its magnitude is fixed by the choice of $|v_{0n}|$ or $|i_{0n}|$ while its phase is fixed by p_{0n}.

The vectors of modal voltages $\boldsymbol{v}_{\mathrm{m}}$ and modal currents $\boldsymbol{i}_{\mathrm{m}}$ satisfy the transmission line equations

$$\frac{\mathrm{d}\boldsymbol{v}_{\mathrm{m}}}{\mathrm{d}z} = -\boldsymbol{Z}_{\mathrm{m}} \boldsymbol{i}_{\mathrm{m}}; \quad \frac{\mathrm{d}\boldsymbol{i}_{\mathrm{m}}}{\mathrm{d}z} = -\boldsymbol{Y}_{\mathrm{m}} \boldsymbol{v}_{\mathrm{m}} \;, \tag{2}$$

where the matrices of modal impedance and admittances per unit length are defined by $\boldsymbol{Z}_{\mathrm{m}} \equiv \boldsymbol{\gamma}\, \boldsymbol{Z}_0$, $\boldsymbol{Y}_{\mathrm{m}} \equiv \boldsymbol{\gamma}\, \boldsymbol{Z}_0^{-1}$, $\boldsymbol{\gamma} = \mathrm{diag}(\gamma_n)$, and $\boldsymbol{Z}_0 = \mathrm{diag}(Z_{0n})$ [1]. The modal equivalent circuit per unit length of the multiconductor line is sketched in the upper part of Fig. 1.

When a finite number of the discrete modes are excited in the line, the total complex power p carried in the forward direction is

$$p = \int \boldsymbol{E}_{\mathrm{t}} \times \boldsymbol{H}_{\mathrm{t}}^{\,*} \cdot \boldsymbol{z}\, \mathrm{d}S = \sum_{n,k} \frac{v_{\mathrm{m}n}}{v_{0n}} \frac{i_{\mathrm{m}k}^{\,*}}{i_{0k}^{\,*}} \int \boldsymbol{e}_{\mathrm{t}n} \times \boldsymbol{h}_{\mathrm{t}k}^{\,*} \cdot \boldsymbol{z}\, \mathrm{d}S = \boldsymbol{i}_{\mathrm{m}}^{\,\dagger}\, \boldsymbol{X}\, \boldsymbol{v}_{\mathrm{m}}, \qquad \textbf{(3)}$$

where the superscript † indicates the Hermitian adjoint (conjugate transpose), the elements of the cross-power matrix $\boldsymbol{X}$ are defined by $X_{nk} \equiv (v_{0k} i_{0n}^{\,*})^{-1} \int \boldsymbol{e}_{\mathrm{t}k} \times \boldsymbol{h}_{\mathrm{t}n}^{\,*} \cdot \boldsymbol{z}\ \mathrm{d}S$, $X_{nn} = 1$, and the integrals are performed over the entire transmission-line cross section [1].

CONDUCTOR REPRESENTATION

Since every excited mode in a multiconductor transmission line will impress a voltage across each of its conductors, the total voltage between any given pair of its conductors will be a linear combination of all of the modal voltages of the excited modes. Likewise the total current in any given conductor will be a linear combination of the modal currents. References [1] and [2] refer to these linear combinations of modal voltages and currents as the "conductor" voltages and currents; Ref. [10] compares the modal and conductor representations.

The vectors of conductor voltages $\boldsymbol{v}_{\mathrm{c}}$ and currents $\boldsymbol{i}_{\mathrm{c}}$ of [1] and [2] are defined by $\boldsymbol{v}_{\mathrm{c}} \equiv \boldsymbol{M}_{\mathrm{v}}\, \boldsymbol{v}_{\mathrm{m}}$ and $\boldsymbol{i}_{\mathrm{c}} \equiv \boldsymbol{M}_{\mathrm{i}}\, \boldsymbol{i}_{\mathrm{m}}$, where the matrices $\boldsymbol{M}_{\mathrm{v}}$ and $\boldsymbol{M}_{\mathrm{i}}$ are unitless. The vectors $\boldsymbol{v}_{\mathrm{c}}$ and $\boldsymbol{i}_{\mathrm{c}}$ are "power-normalized" in [1] and [2] so that $p = \boldsymbol{i}_{\mathrm{c}}^{\,\dagger}\, \boldsymbol{v}_{\mathrm{c}}$: this requires that $\boldsymbol{M}_{\mathrm{v}}$ and $\boldsymbol{M}_{\mathrm{i}}$ satisfy $\boldsymbol{M}_{\mathrm{i}}^{\,\dagger} \boldsymbol{M}_{\mathrm{v}} = \boldsymbol{X}$. The vectors $\boldsymbol{v}_{\mathrm{c}}$ and $\boldsymbol{i}_{\mathrm{c}}$ satisfy the transmission line equations

$$\frac{\mathrm{d}\boldsymbol{v}_{\mathrm{c}}}{\mathrm{d}z} = -\boldsymbol{Z}_{\mathrm{c}} \boldsymbol{i}_{\mathrm{c}}; \quad \frac{\mathrm{d}\boldsymbol{i}_{\mathrm{c}}}{\mathrm{d}z} = -\boldsymbol{Y}_{\mathrm{c}} \boldsymbol{v}_{\mathrm{c}}\ , \qquad \textbf{(4)}$$

where the matrices of conductor impedance and admittances per unit length are defined by

$\boldsymbol{Z}_c \equiv \boldsymbol{R}_c + j\omega\boldsymbol{L}_c \equiv \boldsymbol{M}_v\ \boldsymbol{Z}_m\ \boldsymbol{M}_i^{-1}$ and $\boldsymbol{Y}_c \equiv \boldsymbol{G}_c + j\omega\boldsymbol{C}_c \equiv \boldsymbol{M}_i\ \boldsymbol{Y}_m\ \boldsymbol{M}_v^{-1}$ [1]. The conductor equivalent circuit per unit length of the multiconductor line is sketched in the lower part of Fig. 1.

DETERMINATION OF MODAL PARAMETERS FROM $\boldsymbol{Z}_c$ AND $\boldsymbol{Y}_c$

The measurement algorithm uses the procedure outlined in Ref. [1] for determining $\boldsymbol{\gamma}$, $\boldsymbol{M}_v$, $\boldsymbol{M}_i$, and the impedance matrix $\boldsymbol{Z}$ of the multiconductor transmission line from $\boldsymbol{Z}_c$ and $\boldsymbol{Y}_c$. This procedure, which reduces to that used in Ref. [3] for a pair of symmetric coupled microstrip transmission lines, is based on the fact that $\boldsymbol{M}_v$ and $\boldsymbol{M}_i$ diagonalize $\boldsymbol{Z}_c\boldsymbol{Y}_c \equiv \boldsymbol{M}_v\ \boldsymbol{\gamma}^2\ \boldsymbol{M}_v^{-1}$ and $\boldsymbol{Y}_c\boldsymbol{Z}_c \equiv \boldsymbol{M}_i\ \boldsymbol{\gamma}^2\ \boldsymbol{M}_i^{-1}$; the eigenvalues of $\boldsymbol{Z}_c\boldsymbol{Y}_c$ (or $\boldsymbol{Y}_c\boldsymbol{Z}_c$) determine $\boldsymbol{\gamma}$ while the columns of $\boldsymbol{M}_v$ are proportional to the eigenvectors of $\boldsymbol{Z}_c\boldsymbol{Y}_c$ and the columns of $\boldsymbol{M}_i$ are proportional to the eigenvectors of $\boldsymbol{Y}_c\boldsymbol{Z}_c$.

The proportionality constants needed to fix the columns of $\boldsymbol{M}_v$ are determined from the definitions of the modal voltage paths in terms of the conductor paths. The coupled lines we studied support two dominant quasi-TEM modes, which are commonly called the *c* and π modes, and which correspond to the even and the odd mode of the symmetric case, respectively; we assumed that only these two modes were significantly excited in the coupled lines. Thus we fixed the first column of $\boldsymbol{M}_v$, which corresponded to the c mode, by setting M_{v21} equal to 1; this defines the c-mode voltage equal to that between the second microstrip conductor and the ground plane. We fixed the second column of $\boldsymbol{M}_v$, which corresponded to the π mode, by setting $M_{v12} + M_{v22} = -1$; this defines the π-mode voltage equal to the difference of the voltages between the first and second microstrip conductors. These conditions completely determine $\boldsymbol{M}_v$ and are easily extended to other cases.

The proportionality constants needed to fix the columns of $\boldsymbol{M}_i$ are found from the relation

$\boldsymbol{M}_i^{\dagger}\boldsymbol{M}_v = \boldsymbol{X}$, which implies that the product of each column of $\boldsymbol{M}_v$ and the complex conjugate of the corresponding column of $\boldsymbol{M}_i$ must be equal to a diagonal element of $\boldsymbol{X}$, all of which are equal to 1.

Once $\boldsymbol{M}_v$ and $\boldsymbol{M}_i$ are determined we can find all of the modal parameters from $\boldsymbol{Z}_m \equiv \boldsymbol{M}_v^{-1}\,\boldsymbol{Z}_c\,\boldsymbol{M}_i$, $\boldsymbol{Y}_m \equiv \boldsymbol{M}_i^{-1}\,\boldsymbol{Y}_c\,\boldsymbol{M}_v$, $\boldsymbol{Z}_0 \equiv \boldsymbol{\gamma}^{-1}\,\boldsymbol{Z}_m$, and $\boldsymbol{X} = \boldsymbol{M}_i^{\dagger}\boldsymbol{M}_v$. Calculations show that the reciprocity matrix of coupled microstrip lines in the conductor representation is nearly the identity, so we can approximate the diagonal matrix $\boldsymbol{W}_m$ of modal reciprocity factors from $\boldsymbol{W}_m \approx \boldsymbol{M}_v^{t}\,\boldsymbol{M}_i$ [1].

We needed to calculate the full conductor impedance matrix $\boldsymbol{Z}$ of the sections of line during the optimization process to predict the measured two-port impedance matrices from the estimates of $\boldsymbol{Z}_c$ and $\boldsymbol{Y}_c$, which we allowed to vary during the optimization process, and the measured termination impedances. We determined $\boldsymbol{Z}$ from [1]

$$\boldsymbol{Z} = \begin{bmatrix} \boldsymbol{M}_v\,\boldsymbol{Z}_0\coth(\boldsymbol{\gamma}\,l_0)\,\boldsymbol{M}_i^{-1} & \boldsymbol{M}_v\,\boldsymbol{Z}_0\sinh(\boldsymbol{\gamma}\,l_0)^{-1}\,\boldsymbol{M}_i^{-1} \\ \boldsymbol{M}_v\,\boldsymbol{Z}_0\sinh(\boldsymbol{\gamma}\,l_0)^{-1}\,\boldsymbol{M}_i^{-1} & \boldsymbol{M}_v\,\boldsymbol{Z}_0\coth(\boldsymbol{\gamma}\,l_0)\,\boldsymbol{M}_i^{-1} \end{bmatrix}, \qquad \textbf{(5)}$$

where l_0 is the length of the line, $\coth(\underline{\gamma} l_0) \equiv \mathrm{diag}(\coth(\gamma_n l_0))$, and $\sinh(\underline{\gamma} l_0)^{-1} \equiv \mathrm{diag}(1/\sinh(\gamma_n l_0))$.

MEASUREMENT PROCEDURE

Figure 2 illustrates the measurement procedure. It begins with a multiline TRL calibration [11] with reference impedance correction [12] in the microstrip access lines to correct for the imperfections in the analyzer and to remove the effects of the wafer probes, via-hole transitions (not shown), and microstrip access lines used to connect the analyzer to the coupled lines: this eliminates the models of Ref. [3] required to account for the contacts and access lines. The initial reference plane of this calibration is in the middle of the shortest line, marked A in Fig. 2. We move this reference plane to the position marked B in Fig. 2 to determine the impedances of our imperfect loads, which consisted of a section of the access line, a probe, and a coaxial load. We set the calibration reference planes to C of Fig. 2 to measure the two-port impedances of the coupled lines terminated with these imperfect loads. The figure shows only one of the combinations of probe and termination connections we used: the entire set of measurements included all of the possible connections of the probes and terminations.

As explained in the introduction we optimize the values of $\boldsymbol{Z}_c$ and $\boldsymbol{Y}_c$ using the algorithm of Ref. [4] until the measured two-port impedance matrices best agreed in a least-squares sense to the two-port impedance matrices calculated from the four-port transmission line impedance matrix $\boldsymbol{Z}$ of Eq. **(5)**, which is a function of the values of $\boldsymbol{Z}_c$ and $\boldsymbol{Y}_c$ being optimized, and the measured impedances of the terminations connected to the remaining ports.

We apply the optimization in three stages, first without making any assumptions about $\boldsymbol{G}_c$, $\boldsymbol{C}_c$, $\boldsymbol{R}_c$, or $\boldsymbol{L}_c$. We used this first optimization to verify that $\boldsymbol{G}_c$ is small, $\boldsymbol{C}_c$ is nearly frequency independent, and $\boldsymbol{C}_c$, $\boldsymbol{R}_c$, and $\boldsymbol{L}_c$ are symmetric, properties that we also verified with the full-wave calculation method of Ref. [13]. We then set the elements of $\boldsymbol{G}_c$ to 0 and all of the other matrices symmetric, and repeat the optimization to determine the low-frequency limit $\boldsymbol{C}_{0c}$ of $\boldsymbol{C}_c$. We

perform the optimization a final time with $\boldsymbol{C}_c$ set to this low-frequency limit. The corresponding conductor equivalent circuit model of the transmission line used in this final optimization is shown in the lower part of Fig. 1. We found that the noise in $\boldsymbol{R}_c$, $\boldsymbol{L}_c$, and the modal parameters at this last stage of the analysis was somewhat lower than in the earlier stages.

We tested the method with two asymmetric coupled microstrip lines contacted by single-mode access lines fabricated on the same substrate. The coupled lines had widths of 54 μm and 254 μm separated by a gap of 45 μm printed on an alumina substrate with an approximate thickness of 254 μm and lengths of 1 mm, 6 mm, 11 mm, 16 mm, and 21 mm. Their conductor metalization had a measured thickness of 1.8 μm and measured dc conductivity of $3.3 \times 10^7\ \Omega^{-1} \cdot m^{-1}$.

The procedure ignores coupling between the access lines and parasitics at the junction between the access and coupled lines (point C of Fig. 2). For this reason we constructed the access lines at 90° angles to reduce coupling between them, as illustrated in the figure. The access lines also form an abrupt connection to the conductors of the asymmetric coupled line to reduce parasitics there.

Figure 3 shows elements of $\boldsymbol{L}_c$ in solid lines determined by the analysis. The measurements and calculations agree closely and display clearly the anticipated rise at the low frequencies due to the internal inductance of the conductors.

MEASUREMENTS OF MODAL QUANTITIES

Figures 4 and 5 show modal quantities measured by the procedure. The figures show that the conductor and modal quantities compare reasonably well to calculations using the full-wave method of Ref. [13]. For the calculations we assumed that the substrate had a dielectric constant of 10 and was lossless.

We found that the calculations shown in Fig. 4 were quite sensitive to the size of the artificial magnetic box placed around the lines. While increasing the size of this box improved agreement with the measurements it also slowed solution time. The calculations shown in the figure correspond to a 2854 μm wide by 1460 μm high box, the largest box we were able to simulate with our computer. Extrapolations based on the smaller magnetic boxes we used indicated that the remaining systematic offsets between the numerical and measured results in figures 4 are due in large part to the box.

Reference [5] shows that the discrepancy between the measured and calculated modal cross-powers in Fig. 5 are due to neglecting transition parasitics in the measurement procedure reported here. Despite the discrepancies, Fig. 5 clearly shows that, as predicted by Ref. [14], the modal cross-powers are significant at low microwave frequencies and cannot be ignored in the analysis. Reference [15] shows that the elements of $\boldsymbol{M}_v$ and $\boldsymbol{M}_i$ change in the region where the modal cross-powers become significant; methods such as that of [3], which assume these quantities to be frequency independent, will fail there.

CONCLUSION

We presented a method for the measurement and characterization of lossy asymmetric printed multiconductor transmission lines, important components in electronic packages. The method not only determines the matrices of transmission line capacitance, conductance, inductance, and resistance per unit length in the conductor representations of [1] and [2], but all of the modal quantities, including the modal propagation constants, characteristic impedances, and cross-powers.

The method is based on rigorous relations between the transmission lines conductor

representation, its modal representation, and its impedance matrix. This allows it to be used to characterize lossy asymmetric coupled lines in which the modal cross powers are significant and the relationships between the modal and conductor voltages and currents are complex and frequency dependent.

In our experiments transition parasitics were small. However Ref. [5] shows that the method can also be adapted to de-embed transition parasitics between the analyzer reference planes and multiconductor transmission lines. Although not demonstrated here the method should also be applicable to transmission lines with more than three conductors.

ACKNOWLEDGMENTS

The author appreciates the contributions of Stefaan Sercu and Luc Martens at the University of Ghent in Ghent, Belgium, who made possible the measurements reported here.

REFERENCES

[1] D. F. Williams, L. A. Hayden, and R. B. Marks, "A complete multimode equivalent-circuit theory for electrical design," to be published in *J. Res. Natl. Inst. Stand. Technol.*

[2] N. Faché and D. De Zutter, "New high-frequency circuit model for coupled lossless and lossy waveguide structures," *IEEE Trans. Microwave Theory Tech.*, pp. 252-259, March 1990.

[3] T. Winkel, L.S. Dutta, H. Grabinski, E. Grotelueschen, "Determination of the Propagation Constant of Coupled Lines on Chips Based on High Frequency Measurements," *IEEE Multi-Chip Module Conf. Dig.*, Santa Cruz (CA), pp.99-104, 6-7 Feb., 1996.

[4] P.T. Boggs, R. H. Byrd, and R. D. Schnabel, "A stable and efficient algorithm for nonlinear orthogonal distance regression," *SIAM J. Sci. and Stat. Comp.*, pp. 1052-1078, Nov. 1987.

[5] D. F. Williams, "Embedded multiconductor transmission line characterization," *IEEE International Microwave Symp. Dig.*, paper TH4D-2, June 10-12, 1997.

[6] R. E. Collin, *Field Theory of Guided Waves*. New York: McGraw-Hill, 1960.

[7] G. Goubau, "On the excitation of surface waves," *Proc. I.R.E.*, pp. 865-868, July 1952.

[8] R. B. Marks and D. F. Williams, "A general waveguide circuit theory," *J. Res. Natl. Inst. Stand. Technol.*, pp. 533-561, Sept.-Oct. 1992.

[9] J. R. Brews, "Transmission line models for lossy waveguide interconnections in VLSI," *IEEE Trans. Electron Dev.*, pp. 1356-1365, 1986.

[10] D. F. Williams, "Calibration in Multiconductor Transmission Lines," *48th ARFTG Conference Dig.* (Orlando, FL), Dec. 4-6, 1996.

[11] R. B. Marks, "A Multiline Method of Network Analyzer Calibration," *IEEE Trans. on Microwave Theory and Tech.*, pp. 1205-1215, July 1991.

[12] R. B. Marks and D. F. Williams, "Characteristic Impedance Determination using Propagation Constant Measurement," *IEEE Microwave Guided Wave Lett.*, pp. 141-143, June 1991.

[13] W. Heinrich, "Full-wave analysis of conductor losses on MMIC transmission lines," *IEEE Trans. Microwave Theory Tech.*, pp. 1468-1472, Oct. 1990.

[14] D. F. Williams and F. Olyslager, "Modal cross power in quasi-TEM transmission lines," *IEEE Microwave Guided Wave Lett.*, pp. 413-415, Nov. 1996.

[15] D. F. Williams, "Calibration in multiconductor transmission lines," *48th ARFTG Conf. Dig.*, pp. 46-53, Dec. 5-6, 1996.

FIGURES

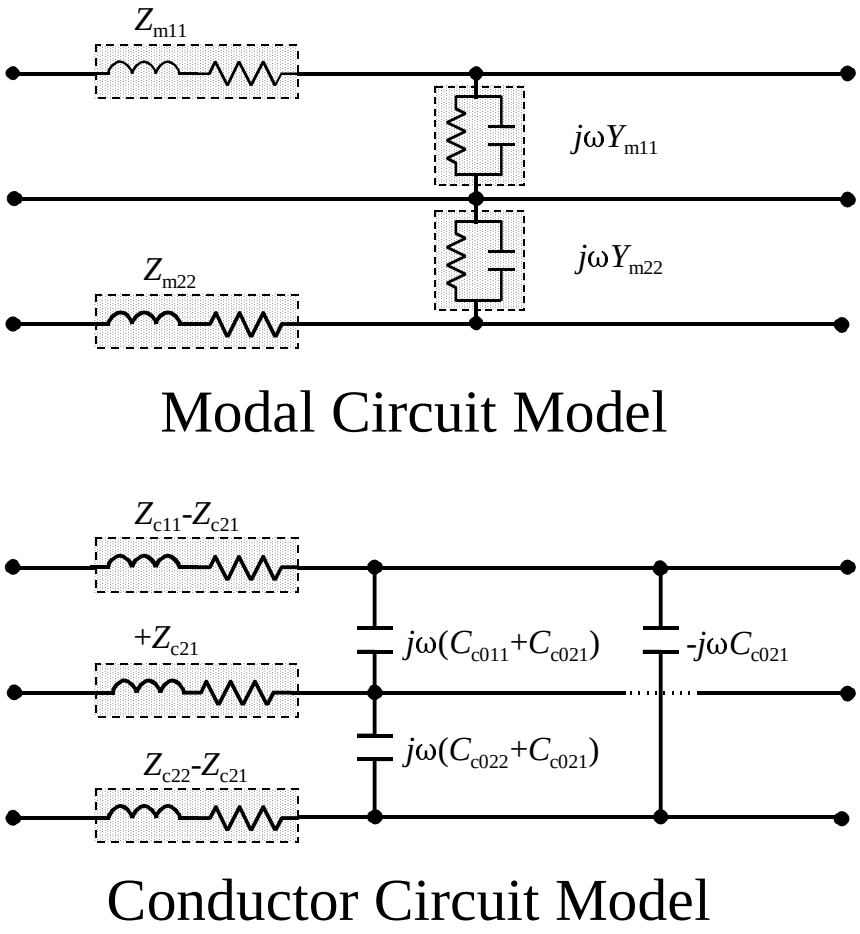

Figure 1. The modal and conductor equivalent circuit models per unit length of transmission line. Only two modes are assumed to be excited in the line. c:\dr\coupled\both.wpg

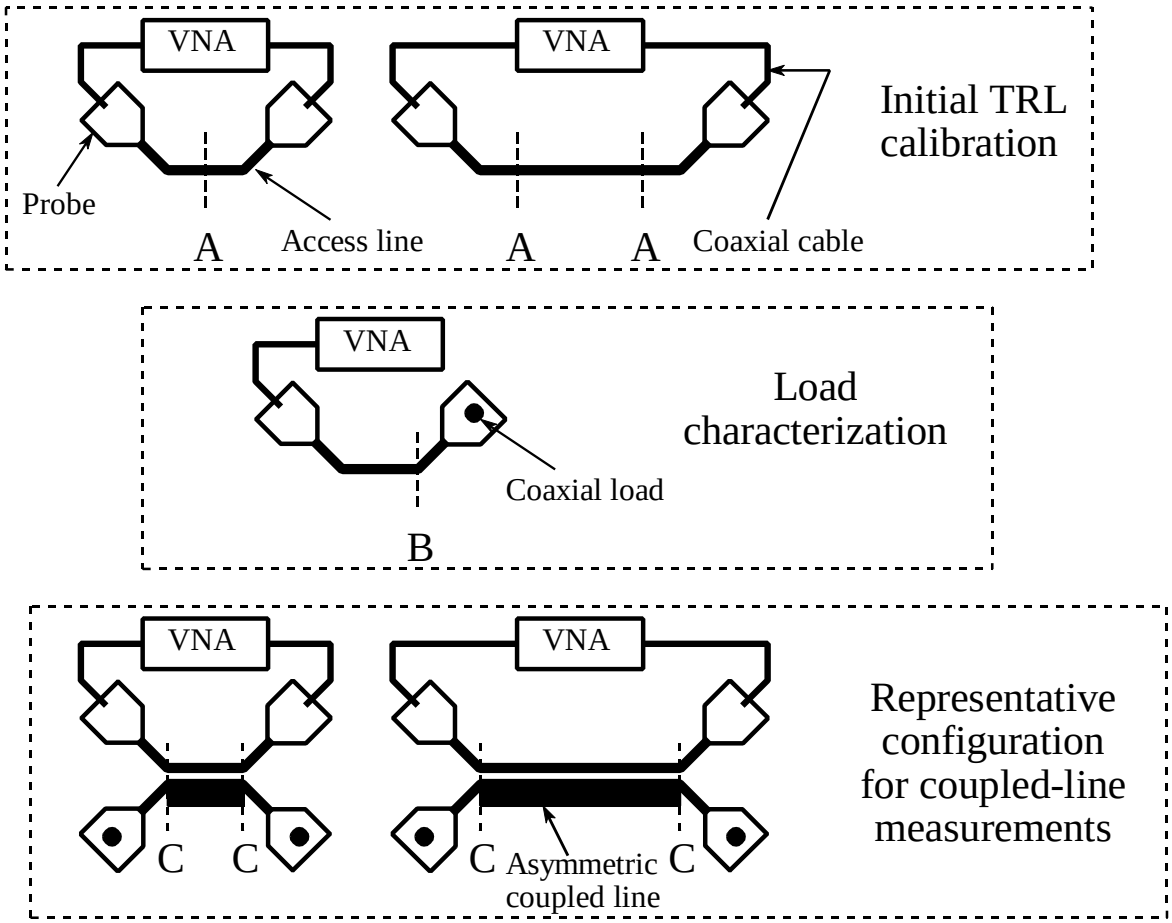

Figure 2. A schematic representation of the measurement artifacts and procedure. Coaxial cables connect the vector network analyzer (VNA) to the ground-signal-ground probes. The probes contact the center conductor of the access lines directly; the ground contact is made with metallized via-holes. c:\dr\coupled\multimod\fig1.wpg

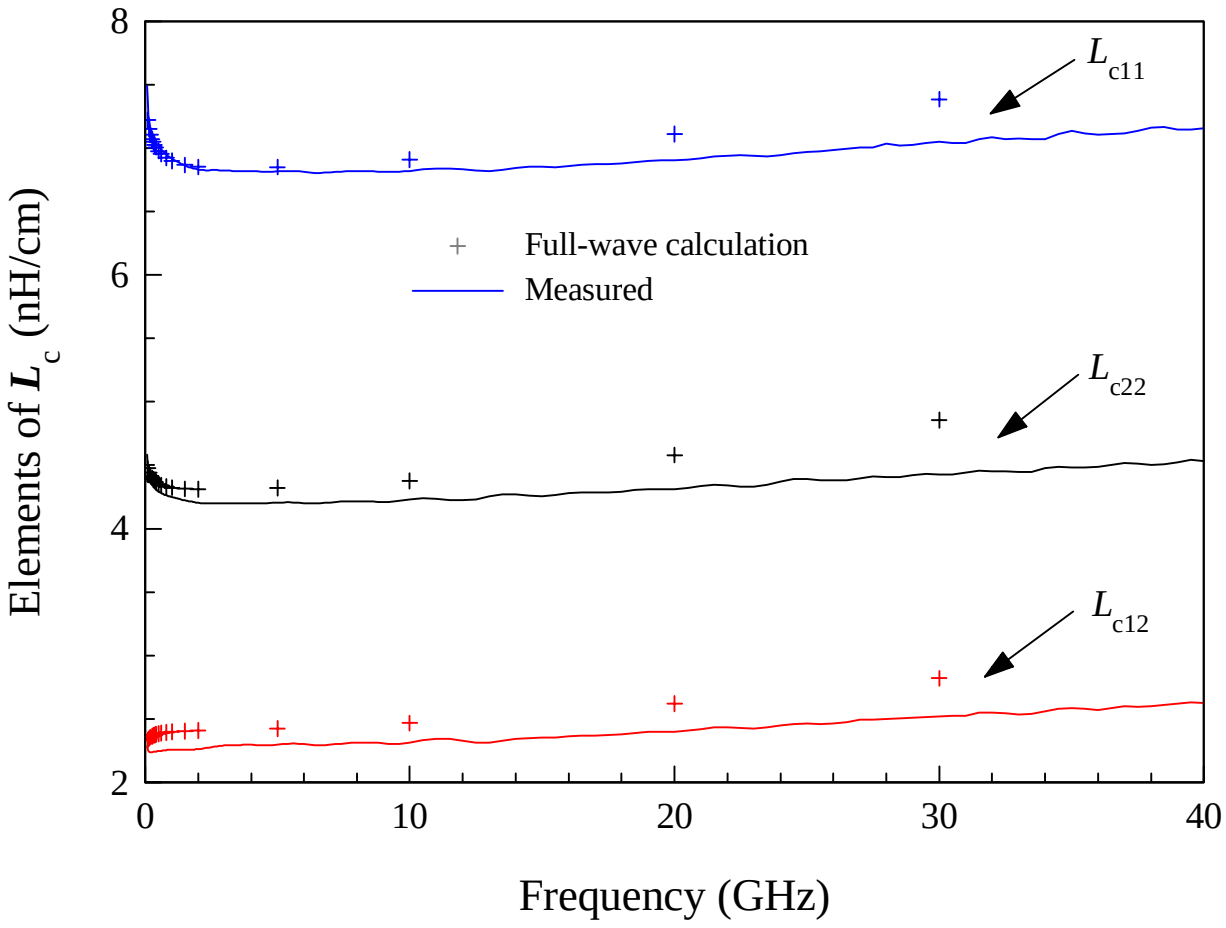

Figure 3. The elements of $\boldsymbol{L}_c$. Solid lines refer to measurements while markers indicate values from the full-wave calculation method of [13].c:\htb386\coupled\asym\plots\l.plt

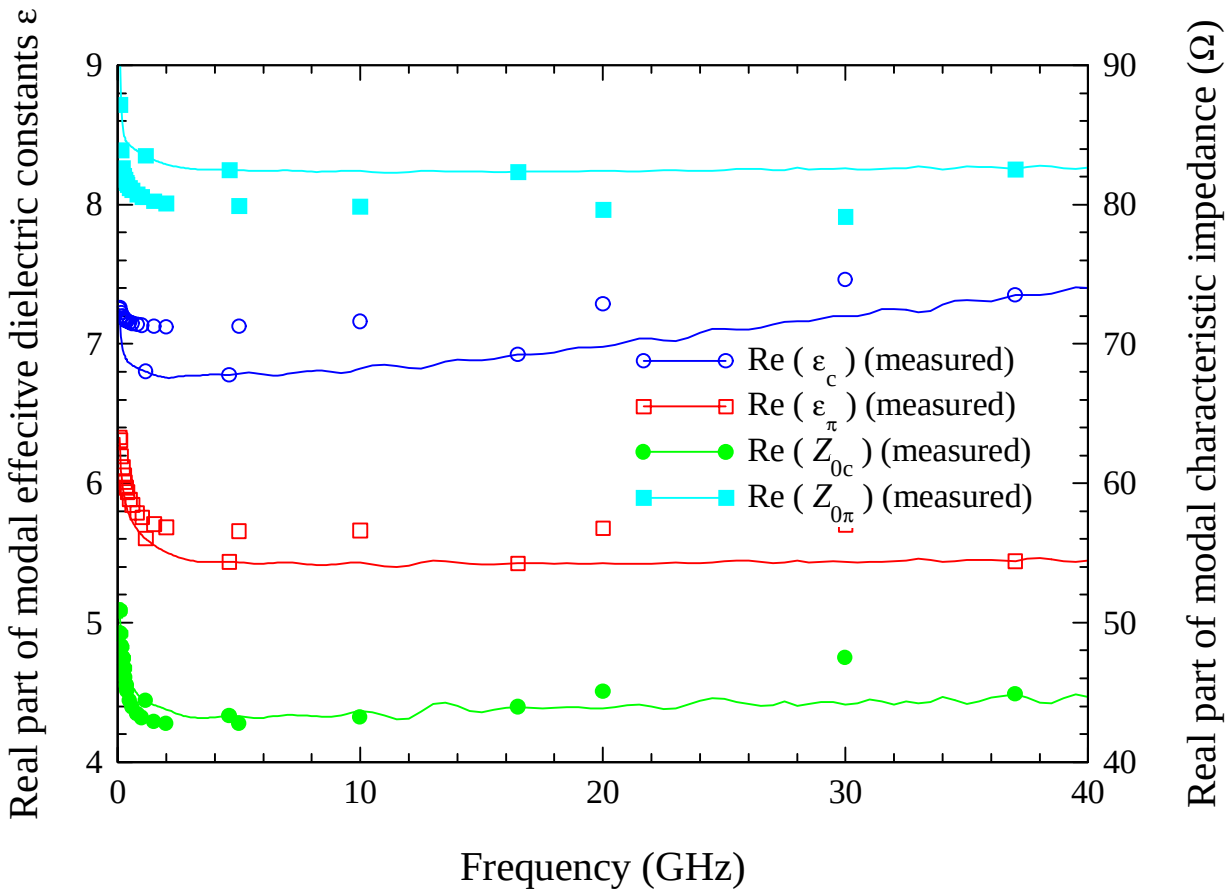

Figure 4. The real part of the measured effective dielectric constants and characteristic impedances of the c and π modes. Solid lines with markers refer to measurements. Markers with no lines indicate values from the full-wave calculation method of [13].

c:\htb386\coupled\asym\plots\all.plt

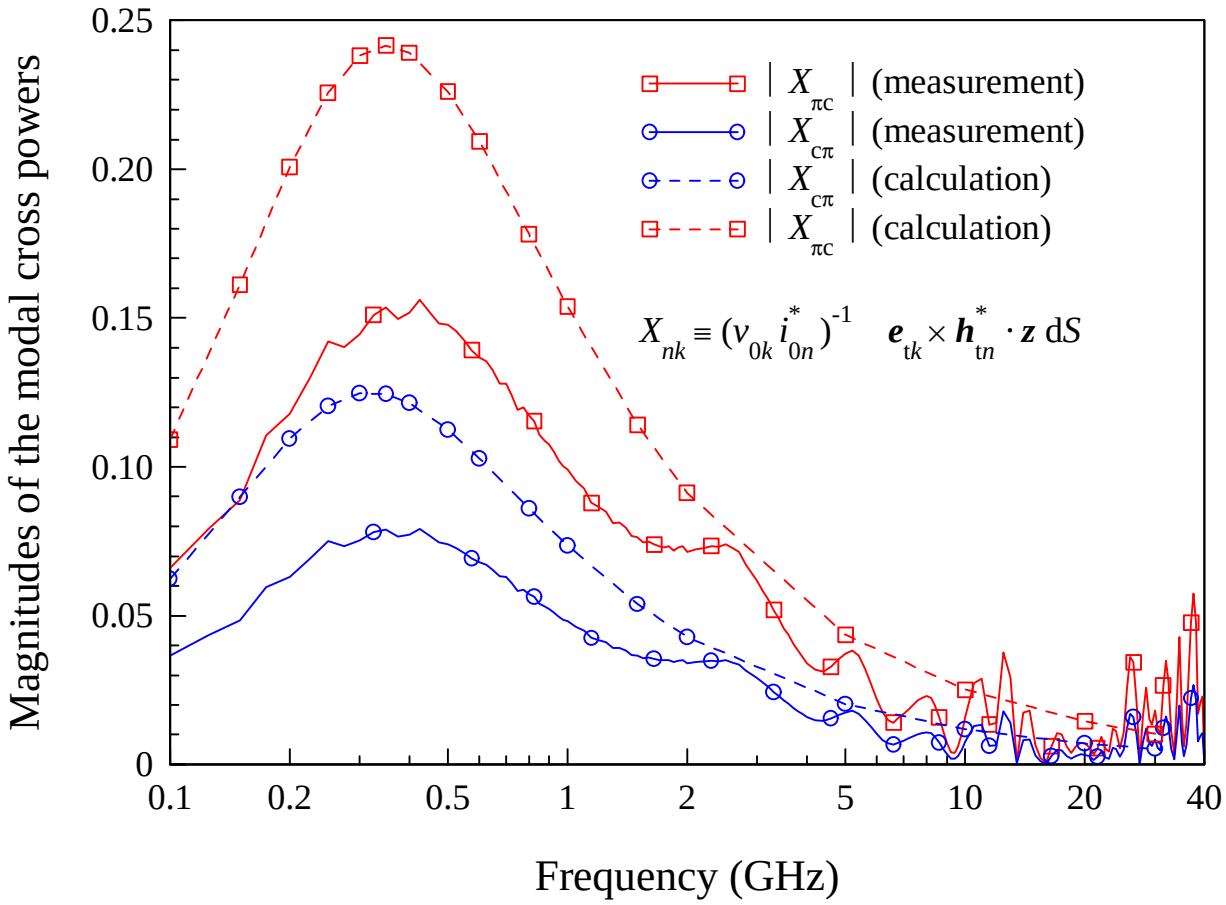

Figure 5. The measured magnitudes of the off-diagonal elements of the modal cross-power matrix ***X***. Solid lines refer to measurements, dashed lines refer to values from the full-wave calculation method of [13]. c:\htb386\coupled\asym\plots\x.plt